06.5;09.1;15.2

Synthesis and diameter distribution approach of vertically aligned carbon nanotubes array

© N.V. Lyanguzov, E.V. Nikitina, V.S. Sim

Southern Federal University, Rostov-on-Don, Russia
E-mail: n.lianguzov@mail.ru

Received August 30, 2021
Revised December 13, 2021
Accepted January 24, 2022

Vertically aligned carbon nanotubes arrays were synthesized via catalytic chemical vapor deposition technique. An opportunity to decreasing of acetylene as a carbon precursor contain down to 0.2% was demonstrated. An iron acetate as an alternative catalyst was proposed. Diameters of carbon nanotubes were estimated by them Raman spectra. Considering resonant behavior of radial breathing modes and them significant environment influencing, an approach based on a profile analyzing of *G*-band was offered to revel of nanotubes diameter distribution features.

Keywords: carbon nanotubes, chemical vapor deposition, Raman spectroscopy, radial breathing modes, *G*-band.

DOI: 10.21883/TPL.2022.04.53164.19008

Vertically aligned carbon nanotube (VA-CNT) arrays are a promising material for the fabrication of cold cathodes [1], electrochemical cells [2], and frequency-selective surfaces [3]. Catalytic chemical vapor deposition (CCVD) with a specific sequence of process operations is the most widespread technique for VA-CNT synthesis [4–7]. Surface-oxidized silicon wafers are commonly used as substrates. A buffer Al_2O_3 layer, which prevents the agglomeration of particles of a catalytic agent (CA), is deposited onto them with the use of various vacuum sputtering techniques. A CA (iron or other 3*d* elements) layer is deposited next. In the process of synthesis, the reaction gas mixture (RGM) of a carrier gas (Ar or He), a reducer (H_2 or NH_3), and a carbon source (C_2H_4 or C_2H_2) is fed into the reactor. The optimum growth temperature falls within the range of 700−800°C. Specifically, it was found that the VA-CNT yield tends to increase if the CA annealing time increases [4] to 15 min. When the concentration of H_2 in the reaction medium grows to 30% [5], the formation of amorphous carbon gets suppressed, while the CA activity increases. This results in the synthesis of high-quality VA-CNTs with a height up to 4 mm. Cobalt was used as an example CA to demonstrate that its preliminary annealing in vacuum contributes to an increase in the CNT yield compared to the yield in the case of annealing in a saturated reducing medium (NH_3) [6]. It is also possible to maximize the CA activity by introducing small controlled amounts of water vapor into the RGM [7].

The aim of the present study is to optimize the processes of synthesis of VA-CNT arrays and analyze the diameter distribution of nanotubes in arrays based on the measured Raman spectra.

Si (111) wafers with a thin (~ 30 nm) SiO_2 surface layer were used as substrates. A thin (10 nm) Al_2O_3 layer was deposited onto them. This was done by centrifuging a droplet of an aluminum oxalate solution in deionized water (the concentration was 0.1 mol/l) at a rotation rate of 1500 rpm and subsequent annealing in air at a temperature of 800°C for 5 min. The CA precursor (ferric acetate) was then deposited by dipping the substrates in its solution in ethanol (the concentration was 0.01 mol/l) and drying in air. The following gases with the corresponding volume flow fractions were introduced into the RGM: H_2 — 25%, C_2H_2 — x%, and Ar — $(75 - x)$%. The value of x varied: 10, 5, 1, and 0.2%. The overall maximum flow was 1000 sccm. The gas flowed freely and under atmospheric pressure. The prepared substrates were loaded into the synthesis reactor, the reactor was sealed, and the residual atmosphere was evacuated. With a mixture of Ar and H_2 flowing, the substrates were transferred quickly with the help of a manipulator into a region of the reaction volume heated to 800°C and were kept there for 5 min. At the next step, C_2H_2 was introduced into the RGM, and the VA-CNT synthesis proceeded further for 10 min. The synthesis was terminated by cutting off the supply of C_2H_2 and H_2 and removing the sample quickly from the heated reactor region.

The morphology of the synthesized samples was studied using a FE-SEM Zeiss SUPRA 25 scanning electron microscope (SEM) and a JEOL JEM-200F transmission electron microscope (TEM). The products of synthesis in samples fabricated with 10 and 5% of C_2H_2 are submicrometer-scale filaments and particles and a small amount of chaotically oriented CNTs. VA-CNTs were synthesized when the concentration of C_2H_2 was 1 or 0.2%. Each individual CNT was not exactly perpendicular to the surface. They were prone to bending, twisting, bundling, and branching of bundles (see the inset of Fig. 1, *a*) and assumed a complex spatial configuration. Bundles formed columnar micrometer-scale agglomerates, and the trend toward vertical growth of a CNT array as a whole was quite evident. The height of the VA-CNT array above the substrate surface was determined by analyzing the photomicrographs of cleaved end faces of

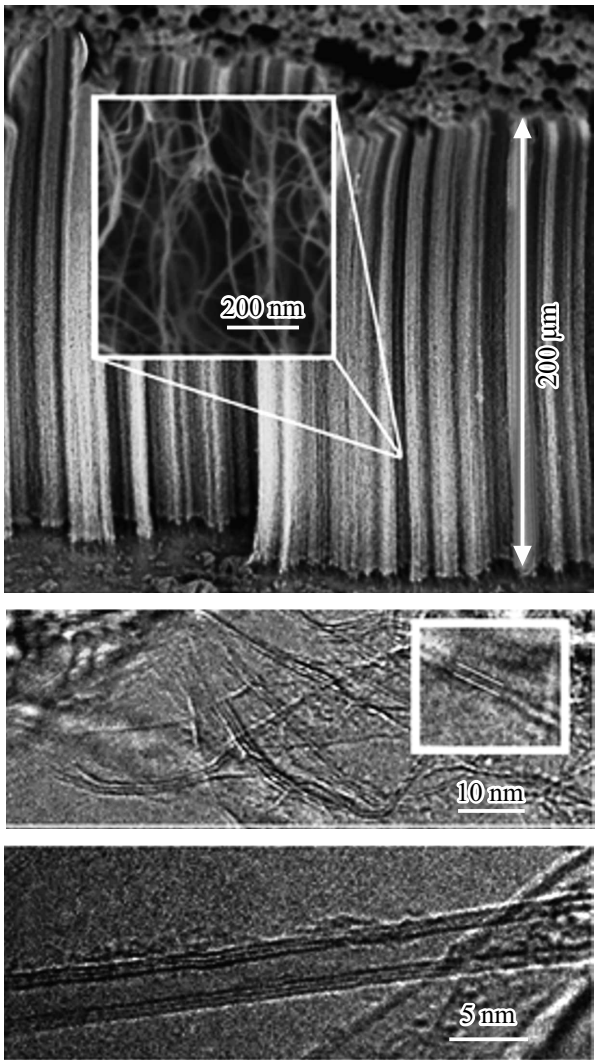

Figure 1. *a* — SEM image of the cleaved end face of a VA-CNT array. A more detailed SEM image is shown in the inset. *b* — TEM image of an individual SWCNT agglomerate. The magnified image of an individual SWCNT is shown in the inset. *c* — TEM image of a triple-walled CNT. TEM images of individual CNTs are recorded with a resolution of 0.2 nm.

samples and was estimated at $\sim 200\,\mu$m (Fig. 1, *a*). With a C_2H_2 concentration of 0.2%, the VA-CNT layer thickness increased at a rate of $\sim 20\,\mu$m/min. The complex spatial configuration of individual CNTs makes it hard to estimate their growth rate. TEM data revealed that more than 90% of CNTs are single-walled (Fig. 1, *b*) and form bundles, which are seen clearly in Fig. 1, *a*. An insignificant amount (less than 10%) of double- and triple-walled CNTs was also detected (Fig. 1, *c*), while multi-walled CNTs were extremely rare.

A Renishaw in Via spectrometer was used to measure the Raman spectra of VA-CNTs under excitation at a wavelength of 514 nm (Ar^+ laser) and 633 nm (He–Ne laser) with a spectral resolution of $\sim 1.5\,\text{cm}^{-1}$. Radial breathing modes (RBMs), which are typical of CNTs, and the *G* band split into TO and LO components were observed. *D* and *D*′ components, which are associated with defects or amorphous carbon particles, were also detected. Their relative intensity decreased sharply when the C_2H_2 concentration set in the process of synthesis dropped to 0.2%.

RBM lines typical of CNTs were observed in the spectral region up to $300\,\text{cm}^{-1}$ (Fig. 2). In accordance with the generalized model [8], the RBM frequency is related to the diameter of single-walled CNTs (SWCNTs) in the following way:

$$\omega_{\text{RBM}} = A(1 + C_e d^2)^{1/2}/d, \qquad (1)$$

where coefficients A and C_e characterize the elastic properties of SWCNTs and their interaction with the environment, respectively. The best fit of ω_{RBM} and d for isolated SWCNTs was observed at $A = 227\,\text{cm}^{-1} \cdot \text{nm}$. The adsorption of atmospheric water molecules [9] at standard conditions yields a value of $C_e \approx 0.65\,\text{nm}^{-2}$. In the case of double- and multi-walled CNTs (DWCNTs and MWCNTs), the RBM frequency also increases due to the interlayer interaction (for example, it increases by as much as $20\,\text{cm}^{-1}$ for DWCNTs with a diameter of ~ 1.5 nm) [10] or due to the adsorption of atmospheric moisture [11]. These interactions have a considerable effect on the energy spectrum of MWCNTs as well [12]. It should also be stressed that, owing to the resonance nature of excitation, the lack of RBM lines at a certain frequency does not imply that the corresponding CNTs are lacking in an array. The estimated diameters of synthesized VA-CNTs are listed in Table 1. The obtained values fall within the range of 0.8–2.05 nm.

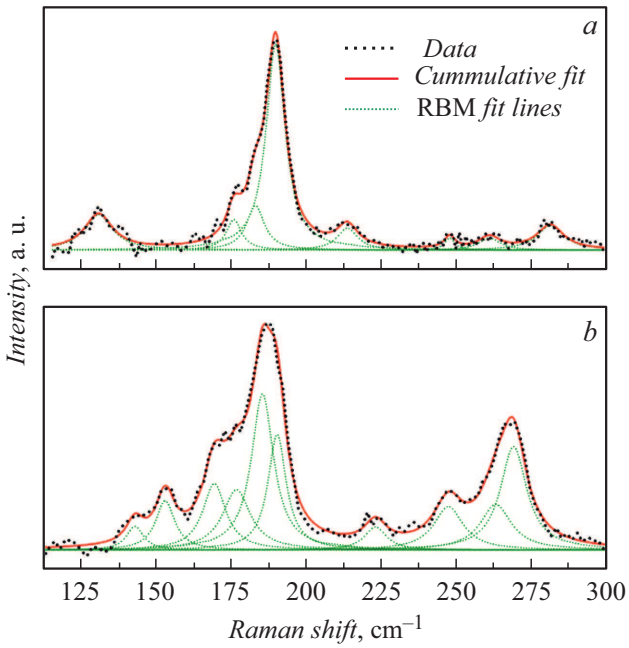

Figure 2. Raman spectra of a VA-CNT array in the RBM region under excitation at a wavelength of 633 (*a*) and 514 nm (*b*). The results of approximation by decomposition into separate Lorentzian profiles are also presented.

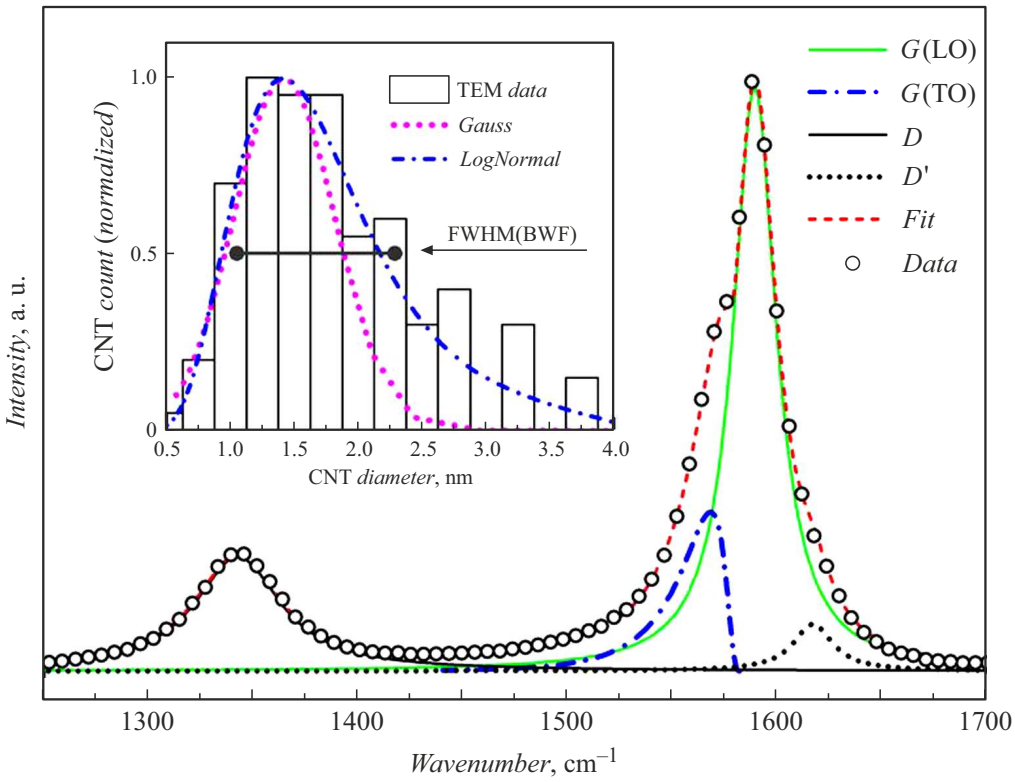

Figure 3. D and G regions of the Raman spectrum of a VA-CNT array under excitation at a wavelength of 514 nm. Single Lorentzian functions with FWHM = 41, 24, and 25 cm^{-1} were used to approximate the D, $G(LO)$, and D' components, respectively. The $G(TO)$ component was approximated with FWHM = 29 cm^{-1} under the assumption that the CNT diameter distribution is lognormal. The histogram of the CNT diameter distribution obtained based on the TEM data is shown in the inset. Its discretization interval of 0.25 nm exceeds the resolution of TEM images used in the statistical analysis. The diameter of an insignificant amount of double- and triple-walled CNTs was determined as the diameter of the outer layer. Curves represent the lognormal and Gaussian distribution functions with parameters obtained as a result of approximation. The line segment corresponds to CNT diameter values calculated based on FWHM in approximation of the $G(TO)$ component with the BWF function.

We then analyzed the G modes of CNTs that are much less sensitive to the environment and less resonant in their excitation nature than RBMs [10,11]. Figure 3 presents the experimental Raman spectrum of the G region of VA-CNTs and the results of its decomposition into constituent profiles. A single Lorentzian function with a full width at half maximum (FWHM) of 24 cm^{-1} was used for approximation of the $G(LO)$ component. The close reproduction of the experimental spectrum agrees here with the assumption that SWCNTs constitute an overwhelming majority of nanotubes. If a considerable fraction of MWCNTs was present, the $G(LO)$ component profile would likely have a complex asymmetric shape due to the frequency shift induced by the interlayer interaction [13]. The $G(TO)$ component is asymmetric in nature. In a CNT array, it could be regarded as a superposition of the corresponding modes of individual CNTs with different diameters at different frequencies. Therefore, the $G(TO)$ component profile should be a convolution of the spectral response of each CNT with the statistical CNT diameter distribution function. The dependence of the spectral position of the $G(TO)$ mode on the CNT diameter [10] is given by [14]

$$\omega_{TO}(d) = A - B/d^2, \qquad (2)$$

where $A = 1582\ cm^{-1}$ and $B = 27.5\ nm^{-2}$. It follows from (2) that a certain number of CNTs with a larger diameter in a CNT array produces a greater contribution to the $G(TO)$ profile intensity at a higher frequency than the same number of nanotubes with a smaller diameter at a lower frequency. In our view, this is the reason why the $G(TO)$ profile extends asymmetrically into the low-frequency spectral region. The asymmetric Breit–Wigner–Fano (BWF) function may be used to approximate the $G(TO)$ component. This provides a close match to the observed spectrum in the low-frequency region [15], but has no clear physical meaning. Indirect estimation based on (2) for the maximum of the approximated $G(TO)$ component positioned at 1568 cm^{-1} yields a value of 1.4 nm for the maximum of the CNT diameter distribution function. Intersections of the median level of the BWF profile at 1554 and 1578 cm^{-1} yield the values of 0.99 and 2.35 nm, thus providing a distribution function width of 1.36 nm. In order

Table 1. Results of calculation of CNT diameters based on the frequency positions of RBM lines under excitation at two different wavelengths (λ_l).

ω_{RBM}, cm^{-1}	d_1, nm	d_2, nm	d_3, nm
$\lambda_l = 514$ nm			
143	1.587	1.736	1.846
153	1.484	1.603	1.707
169	1.343	1.430	1.523
177	1.282	1.357	1.446
185	1.227	1.292	1.376
190	1.195	1.254	1.335
222	1.023	1.059	1.124
247	0.919	0.945	1.000
262	0.866	0.888	0.938
268	0.847	0.867	0.915
$\lambda_l = 633$ nm			
131	1.733	1.932	2.045
176	1.290	1.366	1.455
183	1.240	1.308	1.393
190	1.195	1.254	1.335
214	1.061	1.102	1.170
248	0.915	0.941	0.996
261	0.870	0.892	0.942
282	0.805	0.822	0.866

Note. The values in columns d_1 and d_2 were calculated using (1) with $C_e = 0$ and $0.65\,nm^{-2}$, respectively. Column d_3 presents the results of calculation for DWCNTs with an interlayer interaction that shifts the RBM frequency upward by $20\,cm^{-1}$: $\omega_{RBM} = 227\,cm^{-1} \cdot nm/d + 20\,cm^{-1}$.

Table 2. Parameters of the CNT diameter distribution obtained in approximation of the G(TO) component with different functions (d_0 is the position of the maximum of the distribution function)

Function	d_0, nm	FWHM(d), nm
Lognormal	1.41	1.24
Gaussian	1.42	0.93
BWF	1.40	1.36

to obtain a CNT diameter distribution in an explicit form, we used formula (2) to express the diameter as a function of frequency:

$$d(\omega_{TO}) = \left(B/(A - \omega_{TO})\right)^{1/2}. \quad (3)$$

Expression (3) was then used as an argument of the distribution function. We considered normal (Gaussian) and lognormal distribution functions and wrote down the expressions for approximation of the G(TO) component based on them and relation (3). The values of key approximation parameters are listed in Table 2 and presented in Fig. 3. These values were next used to plot the CNT diameter distribution functions, and the obtained curves were compared to the histogram of the statistical distribution (inset in Fig. 3). Compared to the Gaussian function, the lognormal distribution function reproduces the statistical data better in the region of larger CNT diameters.

Thus, it was demonstrated that the liquid-phase technique of preparation of catalytically activated substrates allows one to synthesize VA-CNT arrays with a predominant fraction of single-walled CNTs, and a CA annealing time in a reducing medium of 5 min and a hydrogen precursor gas concentration of 0.2% are quite sufficient for their growth. In our view, it is more correct to determine the CNT diameter distribution by analyzing the G region of Raman spectra than by studying the RMB region. If applied here, a lognormal CNT diameter distribution function produces the closest fit to direct statistical data.

Acknowledgments

The authors wish to thank S.B. Rochal (Southern Federal University) for stimulating discussions.

Funding

This study was supported by the Russian Foundation for Basic Research (project No. 18-29-19043 mk).

Conflict of interest

The authors declare that they have no conflict of interest.

References

[1] A. Thapa, Y.R. Poudel, R. Guo, K.L. Jungjohann, X. Wang, W. Li, Carbon, **171**, 188 (2021). DOI: 10.1016/j.carbon.2020.08.081
[2] D.T. Welna, L. Qu, B.E. Taylor, L. Dai, M.F. Durstock, J. Power Sources, **196**, 1455 (2011). DOI: 10.1016/j.jpowsour.2010.08.003
[3] L. Sun, M. Zhu, C. Zhao, P. Song, Y. Wang, D. Xiao, H. Liu, S.H. Tsang, E.H.T. Teo, F. Hu, L. Tu, Carbon, **154**, 503 (2019). DOI: 10.1016/j.carbon.2019.08.001
[4] M.M. Rahman, H. Younes, G. Ni, T. Zhang, A.A. Ghaferi, Mater. Res. Bull., **77**, 243 (2016). DOI: 10.1016/j.materresbull.2016.01.050
[5] Y. Luo, X. Wang, M. He, X. Li, H. Chen, J. Nanomater., **2012**, 542582 (2012). DOI: 10.1155/2012/542582
[6] M. Fouquet, B.C. Bayer, S. Esconjauregui, C. Thomsen, S. Hofmann, J. Robertson, J. Phys. Chem., **118**, 5773 (2014). DOI: 10.1021/jp4085348
[7] D.N. Futaba, K. Hata, T. Namai, T. Yamada, K. Mizuno, Y. Hayamizu, M. Yumura, S. Iijima, J. Phys. Chem., **110**, 8035 (2006). DOI: 10.1021/jp060080e
[8] P.T. Araujo, I.O. Maciel, P.B.C. Pesce, M.A. Pimenta, S.K. Doorn, H. Qian, A. Hartschuh, M. Steiner, L. Grigorian, K. Hata, A. Jorio, Phys. Rev. B, **77**, 241403 (2008). DOI: 10.1103/PhysRevB.77.241403
[9] S. Chiashi, K. Kono, D. Matsumoto, J. Shitaba, N. Homma, A. Beniya, T. Yamamoto, Y. Homma, Phys. Rev. B, **91**, 155415 (2015). DOI: 10.1103/PhysRevB.91.155415
[10] D.I. Levshov, H.N. Tran, M. Paillet, R. Arenal, X.T. Than, A.A. Zahab, Y.I. Yuzyuk, J.-L. Sauvajol, T. Michel, Carbon, **114**, 141 (2016). DOI: 10.1016/j.carbon.2016.11.076

[11] S. Rochal, D. Levshov, M. Avramenko, R. Arenal, T.T. Cao, V.C. Nguyen, J.-L. Sauvajol, M. Paillet, Nanoscale, **11**, 16092 (2019). DOI: 10.1039/C9NR03853A
[12] D.V. Chalin, S.B. Rochal, Phys. Rev. B, **102**, 115426 (2020). DOI: 10.1103/PhysRevB.102.115426
[13] G.M. do Nascimento, T. Hou, Y.A. Kim, H. Muramatsu, T. Hayashi, M. Endo, N. Akuzawa, M.S. Dresselhaus, Carbon, **49**, 3585 (2011). DOI: 10.1016/j.carbon.2011.04.061
[14] H. Telg, J.G. Duque, M. Staiger, X. Tu, F. Hennrich, M.M. Kappes, M. Zheng, J. Maultzsch, C. Thomsen, S.K. Doorn, ACS Nano, **6**, 904 (2012). DOI: 10.1021/nn2044356
[15] A.G. Redina, M.V. Avramenko, N.V. Lyanguzov, Tech. Phys., **66** (3), 445 (2021). DOI: 10.1134/S106378422103021X.